Examining the efficacy of localised gemcitabine therapy for the treatment of pancreatic cancer using a hybrid agent-based model.

Adrianne L. Jenner[1], Wayne Kelly[2], Michael Dallaston[1], Robyn Araujo[1], Isobelle Parfitt[1], Dominic Steinitz[3,4], Pantea Pooladvand[5], Peter S. Kim[5], Samantha J. Wade[6,7], Kara L. Vine[6,7],

[1]School of Mathematical Sciences, Queensland University of Technology, Brisbane, QLD, Australia,

[2]School of Computer Science, Queensland University of Technology, Brisbane, QLD, Australia,

[3]Tweag Software Innovation Lab, London, United Kingdom,

[4]Kingston University, Kingston, United Kingdom,

[5]School of Mathematics and Statistics, University of Sydney, NSW, Australia,

[6]Illawarra Health and Medical Research Institute, Wollongong, NSW, Australia,

[7]School of Chemistry and Molecular Bioscience, University of Wollongong, Wollongong, NSW, Australia,

Abstract

The prognosis for pancreatic ductal adenocarcinoma (PDAC) patients has not significantly improved in the past 3 decades, highlighting the need for more effective treatment approaches. Poor patient outcomes and lack of response to therapy can be attributed, in part, to the dense, fibrotic nature of PDAC tumours, which impedes the uptake of systemically administered drugs. Wet-spun alginate fibres loaded with the chemotherapeutic agent gemcitabine have been developed as a potential tool for overcoming the physical and biological barriers presented by the PDAC tumour microenvironment and deliver high concentrations of drug to the tumour directly over an extended period of time. While exciting, the practicality, safety, and effectiveness of these devices in a clinical setting requires further investigation. Furthermore, an in-depth assessment of the drug-release rate from these devices needs to be undertaken to determine whether an optimal release profile exists. Using a hybrid computational model (agent-based model and partial differential equation system), we developed a simulation of pancreatic tumour growth and response to treatment with gemcitabine loaded alginate fibres. The model was calibrated using *in vitro* and *in vivo* data and simulated using a finite volume method discretization. We then used the model to compare different intratumoural implantation protocols and gemcitabine-release rates. In our model, the primary driver of pancreatic tumour growth was the rate of tumour cell division and degree of extracellular matrix deposition. We were able to demonstrate that intratumoural placement of gemcitabine loaded fibres was more effective than peritumoural placement. Additionally, we found that an exponential gemcitabine release rate would improve the tumour response to fibres placed peritumourally. Altogether, the model developed here is a tool that can be used to investigate other drug delivery devices to improve the arsenal of treatments available for PDAC and other difficult-to-treat cancers in the future.

Author Summary

Pancreatic cancer has a dismal prognosis with a median survival of 3-5 months for untreated disease. The treatment of pancreatic cancer is challenging due to the dense nature of pancreatic tumours which impedes retention of drug at

36   the tumour site. As such, systemic administration of chemotherapies, such as gemcitabine, has a limited efficacy. To

37   overcome this, sustained-release devices have been proposed. These devices are injected locally and release drug

38   slowly over time, providing a concentrated local, sustained drug concentration. To investigate the possible efficacy of

39   these devices, we developed a mathematical model that would allow us to probe treatment perturbations *in silico*. We

40   modelled the individual cancer cells and their growth and death from gemcitabine loaded into the sustained delivery

41   devices. Our platform allows future investigations for these devices to be run *in silico* so that we may better understand

42   the forms of the drug release-profile that are necessary for optimal treatment.

Introduction

44   Inoperable pancreatic ductal adenocarcinoma (PDAC) has a dismal prognosis, with a median survival of 3−5 months

45   for untreated disease [1]. Treatment of PDAC with the chemotherapeutic agent gemcitabine can achieve clinical

46   benefit and symptom improvement in 20−30% of patients [1, 2], although PDAC is still regarded as a chemotherapy-

47   resistant tumour [3, 4]. Gemcitabine is designed to target and kill cancer cells by incorporating into the DNA strand

48   of a PDAC cell allowing only one deoxynucleotide to be incorporated, which prevents strand elongation [5, 6],

49   resulting in cell cycle arrest and subsequent cell death [7, 8]. Despite gemcitabine being established as a standard

50   treatment for advanced PDAC over 20 years, most subsequent large phase III studies have not shown significantly

51   improved survival benefit [9]. Overall prognosis for PDAC has seen little improvement in the last 3 decades, largely

52   due to drug resistance and poor intratumoural drug accumulation.

53   The majority of chemotherapeutics, gemcitabine included, are administered systemically via bolus or

54   infusion intravenous administration. This often results in significant systemic toxicity, with only a fraction of the

55   injected dose reaching the tumour. As such, there has been a growing interest in the development of localized targeted

56   delivery systems which can modify the bio-distribution of drugs and achieve local drug accumulation in the tumour

57   tissue [10–12] (**Figure 1**). For example, drug-eluting polymeric implants are designed to deliver high concentrations

58   of chemotherapeutic drugs directly at the tumour site, overcoming transport and tissues barriers as well as limiting

59   off-target toxicities [13]. Biodegradable implants, can be designed to provide sustained drug release over weeks or

60   months, avoiding repeated external drug dosing, clinic visits and other surgical interventions. The characteristics of

61   these devices make local delivery especially attractive for chemotherapeutics with a narrow therapeutic window or

62   short *in vivo* half-life [14], such as gemcitabine.

63   Drug-loaded polymeric fibres can be prepared by various cross-linking methods and allow for drug molecules

64   to be released in a controlled manner depending on the cross-linking type and methods [15]. Previously, Wade *et al.*

65   [14] showed that wet-spun gemcitabine-loaded alginate fibres inhibited *ex vivo* PDAC spheroid growth and reduced

66   PDAC cell viability compared to gemcitabine delivered as a free drug. In a subsequent study, Wade *et al.* [13, 16]

67   showed that a coaxial fibre formulation, in which the alginate was encased by a polycaprolactone (PCL) shell

68   demonstrated significant *in vivo* antitumour efficacy; however, it is not possible to conclude experimentally whether

69   an alternative release-profile of gemcitabine may be more effective. Fortunately, computational and mathematical

70   modelling is well situated as a predictive tool for quantifying the efficacy of alternative drug release profiles and drug
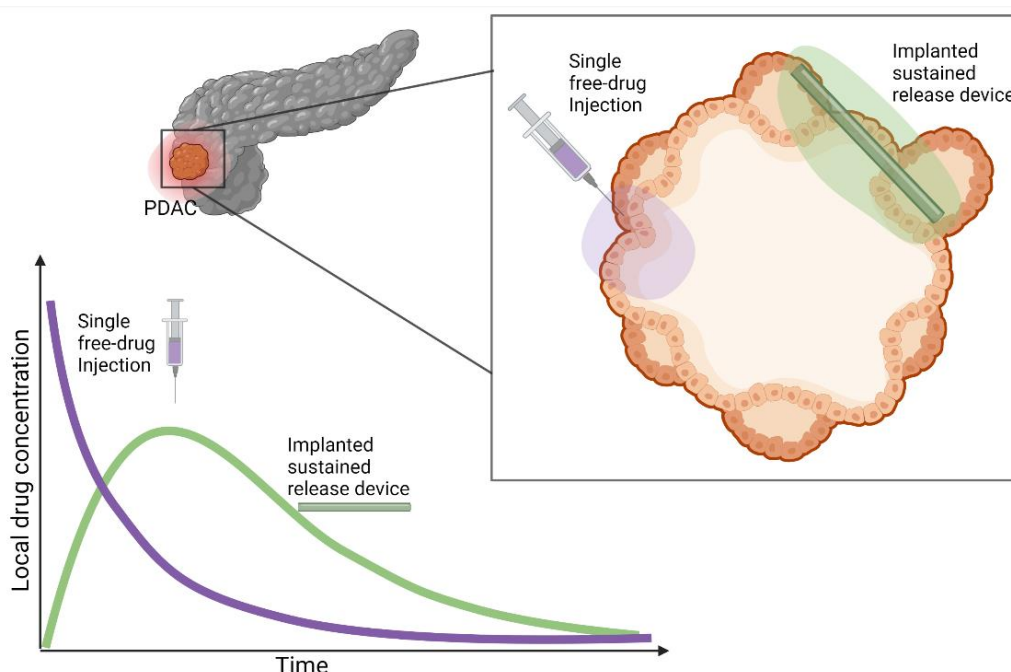
71   administration patterns.

Figure 1 Motivation for sustained-delivery implants for treatment of PDAC. Sustained-delivery implants are a promising treatment methodology over conventional single free-drug intravenous or intrantumoural injections. A hypothetical comparison of drug concentrations at the tumour site under these two protocols is pictured. Systemic injections of anti-cancer drugs often result in a rapid decrease of drug concentration at the tumour site. In comparison, sustained-release mechanisms deliver drug over a prolonged period resulting in a durable drug presence at the tumour site. Created using biorender.com.

Mathematical models have been used to help understand formation and treatment of a range of different cancers for some time now [17–20]. In particular, agent-based models (ABM) have been used extensively in cancer modelling as they allow for the consideration of spatial and phenotypic heterogeneity [21–27] which are known to be major drivers of variations in treatment outcomes. In ABMs, the likelihood of events, such as cell proliferation, movement, death or mutation are modelled as probabilities, allowing the simulation to evolve stochastically in time. Phillips *et al.* [28] presented a hybrid mathematical approach that characterized vascular changes during tumour growth via an ABM, with treatment, nutrient, and VEGF changes captured through a continuum model. Insights on therapeutic failure in immunotherapy have also been provided through an ABM software known as PhysiCell [29, 30]. Oncolytic virotherapy has also been the focus of numerous ABMs [31–35], with an ABM of virotherapy demonstrating that the parameter range leading to tumour eradication is small and hard to achieve in 3D. There have been ABMs developed that specifically focus on pancreatic cancer growth [36, 37]; however, an ABM describing pancreatic cancer growth and treatment with a degradable polymer implant has not yet been developed.

For some time, mathematical models of degradable drug delivery mechanisms have been used to assist in the understanding of polymer degradation, hydrolosis kinetics and the subsequent effect of drug release on the applied system [10, 38–45]. Using mass-balance kinetic equations, McGinty *et al.* [42] investigated the extent to which variable porosity drug-eluting coatings can provide better control over drug release using transport diffusion equations. Their results indicate that the contrast in properties of two layers can be used as a means of better controlling the release, and that the quantity of drug delivered in early stages can be modulated by varying the initial drug distribution.

97　　More recently, Spiridonova *et al.* [46] fitted drug release from polymer microparticles and investigated the effect of

98　　size distribution on diffusional drug release from sustained-delivery systems using a system of partial differential

99　　equations (PDEs). Whilst useful for capturing the drug delivery mechanism, most models of drug-loaded polymers

100　such as these have not examined the influence of changes to drug release profiles on antitumour efficacy or how

101　intratumoural stochasticity impacts drug delivery.

102　　　　In this work, we have developed a hybrid mathematical and computational model of PDAC tumour growth

103　and death from treatment with gemcitabine released from a polymeric fibre. We extended a previously published ABM

104　known as a Voronoi cell-based model (VCBM) [32] to model tumour cell growth and death and coupled this with a

105　PDE model for gemcitabine release from polymeric implants. *In vitro* drug release curves were used to optimise the

106　PDE formulation describing how gemcitabine is released from fibres. A numerical simulation was then used to

107　initialise the parameters in the ABM using *in vivo* control PDAC tumour growth measurements. The potential impact

108　of these fibres on tumour growth and cell death was then investigated with the VCBM-PDE model and improvements

109　on drug release kinetics and fibre placement were suggested. The model was developed as a tool that can be applied

110　to interrogate other cancer therapies using polymeric implants with the goal to improve treatment response for PDAC

111　patients.

Experimental methods

113　*Fibre fabrication and characterisation*

114　Full details for the fabrication and characterisation of alginate fibres loaded with our without gemcitabine are

115　described in Wade *et al.* [13, 14]. Briefly, gemcitabine-loaded alginate fibres had a uniform surface area from $50 -$

116　$120\ \mu m$ in diameter. Fibres displayed different drug release profiles depending on the concentration of polymer

117　used. Fibre diameter also varied depending on the materials used [14].

118

119　*Fibre gemcitabine release kinetics*

120　Full details for the experiments measuring gemcitabine release can be found in Wade *et al.* [14] with brief details here.

121　Gemcitabine-loaded fibres were added to 2mL of simulated body fluid (SBF), Ph 7.4 and incubated at 37°C. At various

122　time points (10, 30, 60, 90 min hourly for 10h and then daily for 3 weeks), buffer solution (200μL) was removed for

123　analysis of gemcitabine release and replaced with fresh SBF. The amount of drug released from alignate fibres was

124　determined using high performance liquid chromatography (HPLC). The amount of gemcitabine released (μg) was

125　calculated by interpolating AUC values from the standard curve using Empower Pro V2 (Waters) software.

126

127　*Implant toxicity in vitro*

128　Gemcitabine loaded fibres were tested for their cytotoxicity against human pancreatic cancer cells (Mia-PaCa-2) cells

129　over 72h. Cells were incubated with 0.5 cm lengths of gemcitabine loaded or non-drug loaded fibre formulation before

130　an endpoint MTS cell viability assay was performed. Results are displayed as a percentage of an untreated control.

131　Experiments were performed in triplicate. Full details for the toxicity experiments can be found in Wade *et al.* [13].

132

133   *In vivo Mia-PaCa-2 cell growth*

134   Animals were subcutaneously inoculated with 100μL suspension of 1×10^6 Mia-PaCa-2 cells in PBS. Tumour

135   volume measurements began when tumours reached a volume of $200\ mm^3$ using

136
$$volume = width \times \frac{length^2}{2}$$

137   where w is the longest tumour measurement and l is the tumour measurement along a perpendicular axis. Tumour

138   volume was measured daily for a duration of approximately 33 days. Full details for this experiment can be found in

139   Wade *et al.* [13]. All animal experiments were conducted in accordance with the NHMRC Australian Code for the

140   Care and Use of Animals for Scientific Purposes, which requires 3R compliance (replacement, reduction, and

141   refinement) at all stages of animal care and use, and the approval of the Animal Ethics Committee of the University

142   of Wollongong (Australia) under protocol AE18/13.

143

144   **Mathematical methods**

145   The model developed for the release of gemcitabine from alginate fibres and the impact on a growing PDAC tumour

146   was formulated in two parts. The first describes the PDE describing the concentration of gemcitabine in the tumour

147   microenvironment (TME) and surrounding tissue over time. The second describes the VCBM [32] that captures the

148   way tumour cells proliferate, move and undergo apoptosis from gemcitabine. All parameters introduced for the model

149   are summarised in **Table S1-S5** in the **Supplementary Tables and Figures** and a schematic for the model is in

150   **Figure 2**.

151   *Model of gemcitabine*

152   To capture the concentration of gemcitabine in the tumour microenvironment, we first considered a 2D rectangular

153   domain with boundary B (**Figure TS1**). Inside this domain, is implanted a gemcitabine drug-loaded fibre which is

154   represented by a vertical line source (**Figure TS2**A and **Figure 2**A). Gemcitabine diffuses from the line source at

155   some time-dependent rate that decreases as the polymeric fibre degradation slows. The gemcitabine concentration in

156   the domain is diffusing and decaying. PDAC cells in the domain are also taking up gemcitabine, removing it from the

157   concentration in the domain. Inside the fibre, we model the diffusion of drug as radially symmetric (**Figure 2**B).

158   We denote the concentration of drug in the TME at position (x, y) by $C(x, y, t)$ and model this concentration

159   by

160
$$\frac{\partial C}{\partial t} = \overbrace{D\nabla^2 C}^{\text{diffusion}} - \overbrace{\lambda C}^{\text{decay}} - \overbrace{\sum_{\text{cells } k} \delta(x - x_k)\delta(y - y_k)v_C W_k C}^{\text{cell uptake}} + \overbrace{\delta(x - x_F)J(y, t)}^{\text{fibre release}}, \tag{1}$$

161   where D is the diffusion coefficient in the TME, and λ is the decay rate of the drug. To model cancer cells taking up

162   gemcitabine, we used $\delta(x)$ which is the Dirac delta function in one-dimension, where (x_k, y_k) is the kth cancer cell's

163   Voronoi centre position in the domain (**Figure S1**), and W_k is the cell's volume. Pancreatic cancer cells take up drug

164   in the domain at a rate v_c. Cell uptake was modelled by point sinks analogous to that in PhysiCell and BioFVM [30,

165   47], where cells are considered discrete "point masses" in the domain that take up drug from a single rectangular

5

166   discretized voxel weighted by the local concentration of drug. We then used a line source at $x = x_F, y_0 \leq y \leq y_0 +$

167   L to model the release of gemcitabine from the polymeric fibre, where y_0 is the location of the bottom of the fibre and

168   L is the fibre length (**Figure TS1**). This line source was represented by a Dirac delta function in one-dimension and

169   the drug diffuses from the line source with flux $J(y,t)$.

170   To derive the flux of drug from the line source, we first assumed that the release of drug from the fibre would

171   be time dependent. As such, we chose to explicitly model a concentration of drug diffusing inside the fibre. We denote

172   the concentration of gemcitabine at radial position r and location (x_F, y) by $F(r, y, t)$ (**Figure TS2** and **Figure 2**A).

173   We model the diffusion and movement of drug inside the fibre assuming radial symmetry. We assumed that diffusion

174   in the radial direction is significantly faster than along the fibre since the radius of the fibre r_{total} is significantly less

175   than the length of the fibre L (**Figure TS1** and **Figure TS2**). This gives

$$\frac{\partial F}{\partial t} = D_F(t) \frac{1}{r} \frac{\partial}{\partial r} \left(r \frac{\partial F}{\partial r} \right), \tag{2}$$

176   where $D_F(t)$ is the time-dependent diffusion of drug inside the fibre. We imposed the continuity condition

$$F(r_{total}, y, t) = C(x_F, y, t), \tag{3}$$

177   so that the diffusion of drug out of the fibre at the line source will depend on the location (x_F, y) and local exterior

178   concentration. The flux out of the line source $J(y,t)$ in **Eq. (1)** can then be approximated from the release of drug

179   across the boundary of the fibre:

$$J(y,t) = \begin{cases} -\dfrac{2\pi r_{total}}{h} D_F(t) \dfrac{\partial F}{\partial r}(r_{total}, y, t) & y_0 \leq y \leq y_0 + L \\ 0 & y < y_0, \quad y > y_0 + L \end{cases}. \tag{4}$$

180   This term is derived by converting the flux out of the radial fibre into the flux represented by the line source in **Eq.**

181   **(1)** and converting to a concentration per surface area where h is the depth of the rectangular region (presumed thing,

182   see **Figure TS1**). Both **Eq. (3)** and **Eq. (4)** are necessary boundary conditions for **Eq. (1)** and **Eq. (2)**. In this way, we

183   assume the concentration is continuous and the flux of the fibre is equal to the flux into the TME, equivalent to a

184   conservation of mass.

185   The diffusivity of the drug, $D_F(t)$, is modeled by the function

$$D_F(t) = \frac{k}{t + \epsilon} + D_{const}, \tag{5}$$

186   where k controls the decay rate to the constant decay rate from the fibre (i.e. how quickly the fibre swells), D_{const} is

187   the constant decay rate from the fibre and ϵ is a tuning constant to provide a finite initial diffusion coefficient, i.e.

188    $D_F(0) = k/\epsilon + D_{const}$. We expect $D_F(0)$ to be initially large (>1) since the polymeric fibre is hydrophilic and drug

189   would immediately diffuse out of the fibre. In addition, some drug is never properly loaded into the fibre and can be

190   released instantaneously. The formalism in **Eq. (5)** was broadly chosen to capture the rapid decline in release as the

191   polymeric fibre degrades. It is possible to model the breakdown of the drug release mechanisms to include device

192   swelling and degradation and for examples of this see [46, 48–50].

193   No-flux boundary conditions on B, the exterior of the TME, are imposed:

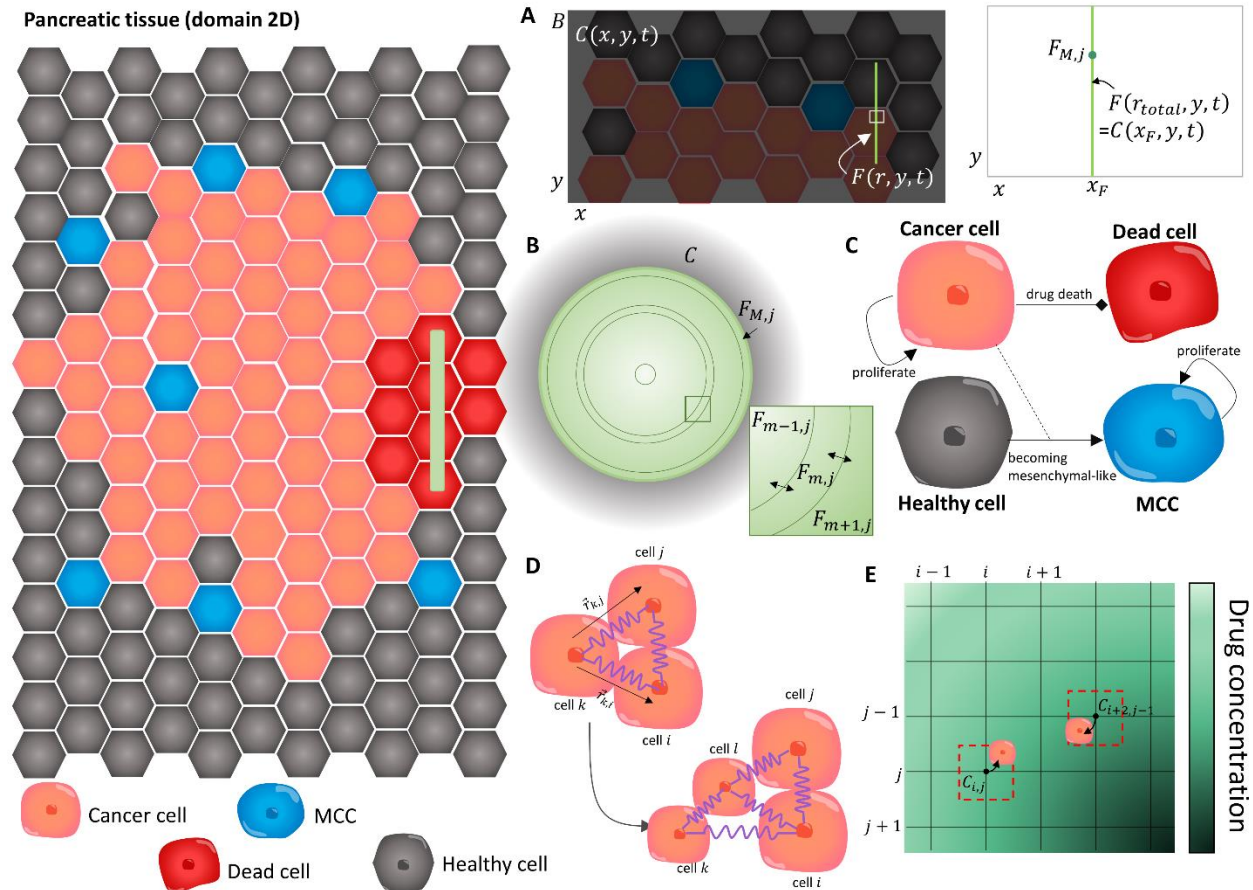194

$$\frac{\partial C}{\partial \vec{n}} = 0$$

6

Figure 2 The main components of the VCBM-PDE model. (A) The concentration of drug in the TME was modelled in a 2D domain bounded by B, where $C(x, y, t)$ was the concentration in the TME at position (x, y). The fibre implant was then placed at a position $x = x_F$ and modelled as a line source. To capture the diffusion of drug from the fibre, we modelled the concentration of gemctiabine inside the fibre $F(r, y, t)$ at radial position r and domain position y where the continuity condition in **Eq. (3)** required equal concentrations at the fibre boundary and at the immedicat local microenvironment, i.e. $F(r_{total}, y, t) = C(x_F, y, t)$. (B) The concentration of gemcitabine inside the polymeric fibres was modelled by radially symmetric difussion **Eq. (2)** using a finite volume method (FVM) discretisation and considering the 2D cylindrical cross section of the fibres which have length L and radius r_{total}. The fibre was discretised into concentric annuli $F_{m,j}$ at annulus m andcross section j, $(i = 0,1, ..., M)$ and the concentration of drug in each annulus $F_{m,j}$ was modelled by considering drug diffusion across the bounadaries (e.g. $F_{m-1,j}$ and $F_{m+1,j}$ flow into $F_{m,j}$ and vice vera). The full discretisation is presented in the **Technical Supplementary Information**). (C) Modelling assumptions for the VCBM were that cancer cells (pink) proliferate and some are able to cause epithelail to mesenchymal transtion and become invasive. We model this transition by assuming cells differentiate into an mesenchymal cancer cell (MCC) with one daughter cell placed on a neighbouring healthy cell. These MCCs cause the break down of surrounding tissue (i.e. replace healthy neighbouring cells with their progeny). Cancer cells can then die through gemcitabine uptake from their local environment. (D) Individual cells were modelled as cell centres connected by springs [32]. The proliferation of a cell introduced a new cell into the lattice network which caused the rearrangement of the cells in the lattice with movement governed by Hooke's law. (E) To simulate the gemcitabine concentration in the TME, **Eq. (1)**, we introduced a FVM discretisation, where the gemcitabine concentration was defined at discrete volumes centered around points in the discretisation. Cells could take up drug from the nearest grid point to their centre, and this concentration was used to determine their likelihood of drug-induced cell-death.

214   where $\vec{n}$ is the outward unit normal on the boundary B (**Figure TS5**). In the case of a fibre implantation, all drug in

215   the domain is initially situated in the fibre:

216
$$F(r, y, 0) = \frac{C_0}{\pi r_{total}^2 L}, \quad C(x, y, 0) = 0,$$

217   where C_0 is the amount of drug in μg, the denominator is the volume of the fibre and there is no drug initially in the

218   domain B. We assume the location of the fibre is fixed in space over the course of the simulation and is not affected

219   by cells around it. For more details on the derivation of the model see the **Technical Supplementary Information.**

220   We solved **Eqs. (1)-(4)** numerically using a Finite Volume approximation. In particular, the diffusion of drug

221   within the fibre, **Eq. (6)**, was solved through discretising the cross section of a fibre into annuli (see **Figure 2**B and

222   the **Technical Supplementary Information**). The model is solved using a finite volume method (FVM)

223   discretization, for examples of this form of discretization in cancer growth and treatment see [51–59].

224

225   *Voronoi Cell-Based Model (VCBM) of pancreatic tumour growth*

226   Agent-based models (ABMs) are primarily used to simulate heterogeneity that arises through stochasticity in cellular

227   interactions. We present an ABM to capture the 2D formation of a pancreatic tumour in the pancreas. Our model

228   extends a Voronoi cell-based model (VCBM) for tumour growth already published in [32]. The model describes how

229   individual cells behave over time by considering their behaviour to be a stochastic process. It uses points as

230   representatives of cell centres and then overlays this with a Voronoi tessellation to define individual cell boundaries.

231   A Voronoi tessellation defines the region of space where the Euclidean distance to a point is less than the distance to

232   any other cell centre in the lattice. Voronoi tessellations have been used to model tissue and cancer cell dynamics for

233   some time [60–64]. Using a Voronoi tessellation for the ABM allows cell morphology to be heterogeneous and not

234   fixed, and the morphology can change with cell movement. The model is solved on a time increment of 1hr to account

235   for the fact that cellular interactions are slow in comparison to drug diffusion (**Figure TS3**). To model pancreatic

236   tumour formation, we assumed the primary functions of pancreatic tumour cells were movement and proliferation.

237   Below are details of the cell types, the model for cell movement and proliferation, a description of the dynamics of

238   tumour mesenchymal cells, the model for cell death and details of how the domain changes as the tumour grows.

239   PDAC cells can acquire mesenchymal-like phenotype properties through a process known as epithelial-

240   mesenchymal transition (EMT) [65–68]. In the EMT process, epithelial elements undergo cytoskeleton remodelling

241   and migratory capacity acquisition due to the loss of intracellular contacts and polarity [66]. This enables the

242   formation of mesenchymal-like cancer cells (MCCs) which have enhanced migratory capacities and invasiveness, as

243   well as elevated resistance to apoptosis [67]. Since there is evidence that EMT plays an important role in PDAC

244   progression [65–68], we have introduced this cell type into the model.

245   We considered four main cell types in the model: healthy pancreatic cells, PDAC cells, MCCs and dead cells

246   (cancer cells that have experienced drug-induced death), see **Figure 2**C. The initial tissue comprised of healthy cells,

247   arranged so that the corresponding Voronoi cells form a hexagonal tessellation, analogous to other work in the

248   literature [69, 70]. To initialise the tumour formation, we removed a healthy cell from the centre of the domain and

249   replaced it with a pancreatic tumour cell (**Figure S1, Supplementary Tables and Figures**). These pancreatic tumour

250   cells could proliferate, die from gemcitabine, or form MCCs. Once formed, these pancreatic stem cells then move and

251   proliferate until they die. Healthy cells are assumed to be able to move or become MCCs.

252   Cell movement is governed by pressure-driven motility, modelled using Hooke's law [32]. Each cell's

253   position is updated by calculating the effective displacement of the cell's lattice point by the sum of the forces exerted

254   on that cell, where force is modelled as a network of damped springs connecting a cell to its nearest neighbours

255   (defined by a Delaunay triangulations). Consider cell k, the displacement of this point in time Δt_{cells} is given by

$$\vec{r}_k(t + \Delta t_{cells}) = \vec{r}_k(t) + \lambda_m \sum_{\forall i} \frac{\vec{r}_{k,i}(t)}{\left|\left|\vec{r}_{k,i}(t)\right|\right|} \left(s_{k,i}(t) - \left|\left|\vec{r}_{k,i}(t)\right|\right| \right), \tag{7}$$

256   where $\vec{r}_k(t)$ is the position of the kth point in the lattice at time t, λ_m is a damping and mobility constant, $\vec{r}_{k,i}$ is the

257   vector between k and i, $s_{k,i}$ is the spring rest length (equilibrium distance) between cell k and i. The introduction of

258   new cells in the lattice through proliferation introduces new spring connections and shortens or extends others,

259   promoting the movement of cells in the environment (**Figure 2**D).

260   Tumour cell proliferation was assumed to be a function of the cell's distance, d_{neut}, to the nutrient source

261   (tumour periphery, i.e. nearest healthy cell centre, see **Figure S3**). The maximum radial distance for nutrient-

262   dependent cell proliferation is d_{max}. Cells that are a further distance from the nutrients than d_{max} enter a quiescent

263   (non-proliferative state), forming what is commonly known as a necrotic core. The probability of a cell dividing p_d in

264   time step Δt_{cells} is given by

$$p_d = \begin{cases} p_0 \left(1 - \dfrac{d_{neut}}{d_{max}} \right) & d_{neut} \leq d_{max} \\ 0 & d_{neut} > d_{max} \end{cases}, \tag{8}$$

265   where p_0 is a proliferation constant derived based on the maximum rate of cell proliferation r (i.e. $p_0 = 1 - $

266    $\exp(-r\Delta t) \approx r\Delta t$). The formalism in **Eq. (8)** is similar to what was used by Kansal *et al.* [71], Jiao and Tarquato [72]

267   and Jenner *et al.* [32]. A cancer cell's ability to proliferate was also based on whether there was enough local space

268   for proliferation to occur. If a cell k proliferates, a new lattice point l is created and the two cells are placed at a

269   distance s/p_{age} from the original proliferating cells position at a rotation $\theta \sim \in U(0,2\pi]$ (**Figure 2**D). To simulate the

270   enlargement and repositioning of the daughter cells, the resting spring length of the connection between k and l

271   linearly increases over time from s/p_{age} to the mature resting spring length s as was formulated in our previous work

272   [32]. Once a cell has proliferated, it takes g_{age} time steps before the daughter cell will try to proliferate again,

273   accounting for G1 phase of the cell cycle where the cell transitions from mitosis M to DNA synthesis S [32]. It is well

274   known that tumours contain highly heterogeneous populations of cells that have distinct reproductive abilities. To

275   account for heterogeneity in the cell cycling, cells sampled the age at birth from a Poisson distribution with mean 50.

276   MCCs are created at the boundary of the tumour with probability p_{MCC}. These cells are created from tumour

277   cells differentiation into a tumour cell and an MCC. We mode their invasive property by placing the daughter cell at

278   the position of a neighbouring healthy cell, removing it from the domain. Through their creation, these MCCs

279   contribute to the degradation of the healthy tissue surrounding the tumour.

280   As in [73–76], we assumed that cancer cells die from gemcitabine contact at a rate described by the Michaelis-

281   Menten term

9

282
$$\beta = \frac{\delta C_{i,j}}{C_{i,j} + IC_{50}},$$

283 where δ is the maximum death rate due to the drug, $C_{i,j}$ is the concentration of drug at the grid position (i,j) in the

284 FVM discretization closest to the cell's centre (**Figure 2**E and the **Technical Supplementary Information**), and IC_{50}

285 is the concentration at which half the effect of the drug is attained. From this, the probability of an individual cell

286 dying can be determined by assuming Prob(cell death)$= 1 - \exp(-\beta \Delta t) \approx \beta \Delta t$. While we chose not to model

287 explicitly the resistance to gemcitabine that cancer cells can develop [3, 4], we believe that by modelling cell death

288 probabilistically we can capture some of the heterogeneity that may exist intratumourally. If a cell dies, then its

289 phenotype changes to be a dead cell and and takes d_{age} hours to disintegrate. To simulate disintegration, at each time

290 increment the spring rest lengths of a dead cell to each of its neighbours, $s_{k,i}$, decreases by $s_{k,i}/d_{age}$.

291   As the tumour grows, the model domain expands. To reduce computational cost, new healthy cells are added

292 to the domain only when a tumour cell's radial distance from empty space is $< 10\mu m$ (**Figure S2 Supplementary**

293 **Tables and Figures**).

294

295 **Numerical simulations and parameter estimation**

296

297 The VCBM-PDE model was written in C++ and simulations called through Matlab 2021b by creating a definition file

298 for the C++ library using *clibgen* and *build* in Matlab 2021b. Code for the model at the various stages (e.g. fibre, single

299 injections) can be found on github (https://github.com/AdrianneJennerQUT/hybrid-VCBM-of-gemcitabine-and-

300 pancreatic-cancer). Full details on all aspects of the code can be found in **Code Documentation**.

301   An approximation for tumour volume was then determined from the 2D simulations using the same formula

302 as the calibre measurements, multiplied by a scalar σ:

303
$$volume = width^2 \times \frac{length}{2} \times \sigma^3$$

304 where $width$ is the longest distance of a cell on the periphery from the centre and $length$ is the distance of the farthest

305 cell from the centre on the radial axis perpendicular to the radial axis of the longest distance (**Figure S5**

306 **Supplementary Tables and Figures**) where σ unit length of the model is equivalent to 1 mm. This calculation choice

307 was made to closely resemble the tumour volume calculation with calibres done *in vivo*. As the size of the

308 computational domain was smaller than the size of the real tumour, the length unit was scaled by σ, which scaled the

309 unit length in the VCBM domain to a comparable mm unit measurement that reduced the computational cost. We

310 chose $\sigma = 0.1728$.

311   All fitting was undertaken using *lsqnonlin* in Matlab 2021b using *pdepe* and *ode45* to simulate the model.

312 Parameters in the model were fit using experimental data or estimated from the literature. To fit the parameters relating

313 to drug release from the fibre we used the *in vitro* drug release experiments. We simplified the model to consider only

314 one cross section, i.e. $F_{m,j} = F_m$, since the outside concentration of drug was independent of location in the absence

315 of cells in the *in vitro* experiment.

10

316   To estimate parameters for the pancreatic cell growth kinetics, we did a large Latin Hypercube sample of the
317   parameter space and determined parameters that resulted in a minimal least squares distance to the *in vivo* control
318   tumour growth measurements. Other parameters were either fixed to previous values in the literature or estimated
319   based on previous work. See **Tables S1-S5** in **Supplementary Tables and Figures** for a full summary of all parameter
320   values and relevant references.

321   **Results**

322

323   *Calibration of drug release kinetics and drug-induced cell death to in vitro measurements*
324   Gemcitabine-loaded fibres were placed in a solution bath and the resulting cumulative concentration of gemcitabine
325   measured (**Figure 3**A). To obtain a model describing the release rate of the drug from the fibre, we fitted parameters
326   from **Eq. (1)-(4)** to these *in vitro* measurements for the release of gemcitabine from 3% alginate 15% PCL fibres [14].
327   Fitting the release curve parameters k, d_{const}, C_0 and A_{out} gave the fit in **Figure 3**B and parameter values in **Table**
328   **S1**. Overall, the model was able to obtain the fit to the data and followed the trend which showed a rapid initial release
329   of gemcitabine followed by a steady-state threshold. We validated the model's predictive capability by also fitting
330   gemcitabine release from 1% and 2% alginate fibres (**Figure S4 Supplementary Tables and Figures**).

331   To assess the efficacy of the drug on inducing death in PDAC cells, cell viability studies were performed
332   using Mia-PaCa-2 cell lines. To model these experiments, we considered a simplified deterministic and spatially
333   independent version of our model with only live cancer cells $P_L(t)$, dead cancer cells $P_D(t)$ and a concentration of
334   drug $C(t)$:

$$\frac{dP_L}{dt} = rP_C - \frac{\delta C}{C + IC_{50}}P_C, \tag{9}$$

$$\frac{dP_D}{dt} = \frac{\delta C}{C + IC_{50}}P_C, \tag{10}$$

$$\frac{dC}{dt} = \mu(t) - \lambda C, \tag{11}$$

335   where r is the exponential proliferation rate of cancer cells *in vitro*, δ is the death rate of cancer cells by gemcitabine,
336   IC_{50} is the drug's half effect concentration, and λ is the decay rate of the drug (**Figure 3**C). To first determine the
337   proliferation rate of pancreatic cancer cells *in vitro*, an exponential growth curve was fit to cell count measurements
338   for Mia-PaCa-2 cells [77] (**Figure 3**D, parameter values **Table S2**) using simple exponential growth (i.e. setting
339    $C(0) = 0$ in **Eq. (9)**). Fixing this growth rate and the estimate for the decay rate of drug, we then determined the
340   antitumour efficacy of gemcitabine-loaded fibres in the cell viability experiments. Cells were treated with aliquots of
341   simulated body fluid from gemcitabine-loaded fibres that had been incubating for 24, 48 or 72 h (**Figure 3**E). To
342   simulate these experiments, the model is solved piecewise such that $\mu(t) = \delta(t - t_{aliquot})C(t_{aliquot})$, where $t_{aliquot}$
343   are the times of the drug administrations. An approximation for the concentration of drug at each time point,
344    $C(t_{aliquot})$, can be determined using the calibrated PDE model for drug release from the fibres. Fitting the drug
345   induced death rate and IC_{50} gave a good approximation to the data (**Figure 3**F). The resulting parameter values from
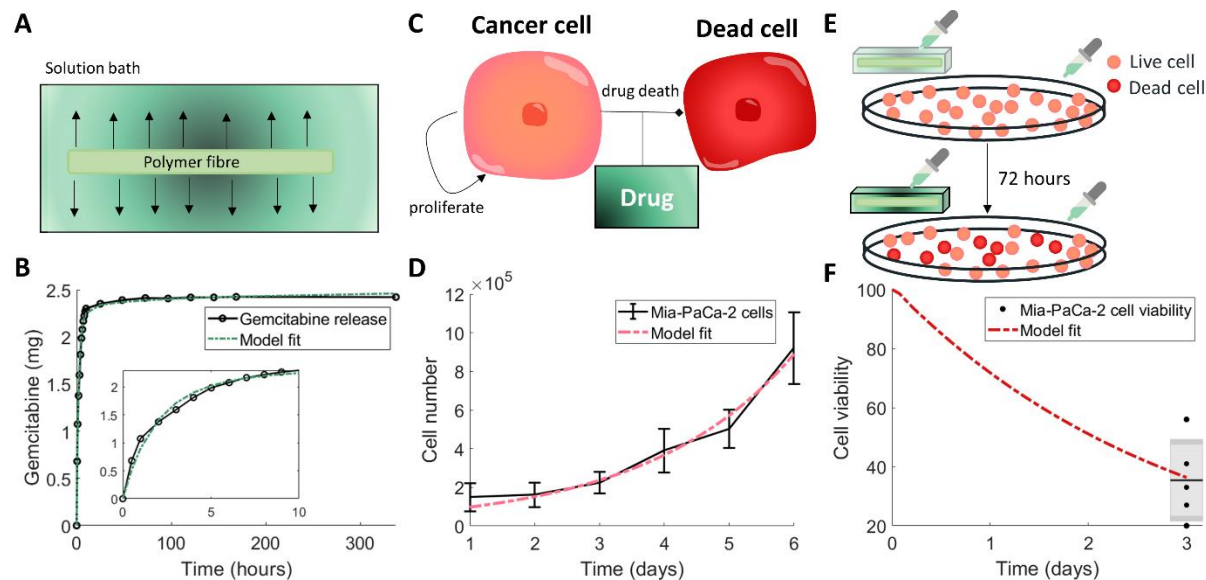346   the fit of the model can be found in **Table S2**.

11

Figure 3 Calibration of model parameters to *in vitro* experiments. (A) Drug release profiles for gemcitabine with 3% alginate 15% PCL were measured by placing the gemcitabine-loaded alginate fibre in a solution bath and measuring the released drug concentration over time. (B) The drug concentration in the solution bath (black) was used to fit model parameters for the drug release from the fibre (green). Resulting parameters are in **Table S1**. (C) The drug-induced death rate of pancreatic cancer cells was determined by simplifying the full model assumptions to consider a homogeneous model for live cancer cells $P_L(t)$ that were proliferating and dying (become dead cells $P_D(t)$) through the effect of the drug gemcitabine $C(t)$, **Eqs. (9)(11)**. (D) Fitting an exponential growth curve to Mia-PaCa-2 cell proliferation *in vitro* [77] gave the growth rate of cells r. Values are the mean±std. (E) To measure the efficacy of the protocol, the cell viability was determined after aliquots from drug released from gemcitabine-loaded fibre were placed in a well with proliferating Mia-PaCa-2 cells at 24, 48 and 72 hours. (F) The resulting cell viability at 72 hours from the experiment depicted in (E) was used to fit the drug-induced cell death rate (**Eq. 9-11**). The data is plotted as a box and whisker plot. Resulting parameters for (D) and (F) are in **Table S2**.

Calibration and sensitivity of pancreatic tumour growth

The VCBM simulation of pancreatic tumour growth in the absence of treatment depicts invasive and disorganised movement of cancer cells into surrounding healthy tissue (**Figure 4**A). To calibrate tumour growth parameters in the model, we used an exhaustive numerical search of the parameter space using a Latin Hypercube Sampling for g_{age}, d_{max}, p_0 and p_{MCC}, where we were minimising the least squares of the simulation with the *in vivo* tumour volume of Mia-PaCa-2 cells over 33 days (**Figure 4**B, **Table S3**). To obtain an understanding of the stochasticity in our model, we fixed the parameter values obtained and we simulated the model 100 times and plotted the tumour volume over 33 days. From **Figure 4**B, while the growth is varied at points, there are no distinct outliers or unusual tumour growth rates, and the standard deviation throughout the entire period of observation remains small. In addition, the simulations sit within the *in vivo* tumour growth measurements for pancreatic cancer growth. The histogram for the number of MCCs across the simulations (**Figure 4**C) shows only a small number of MCCs are created over the 33 days of growth, which is realistic when considering the ratio between a single cell agent in the model and a real cell in a biological tumour and which matches findings that MCCs will compose only a small subset of the tumour [78–80].

To analyse the drivers of pancreatic tumour growth dynamics in our model, we conducted a detailed
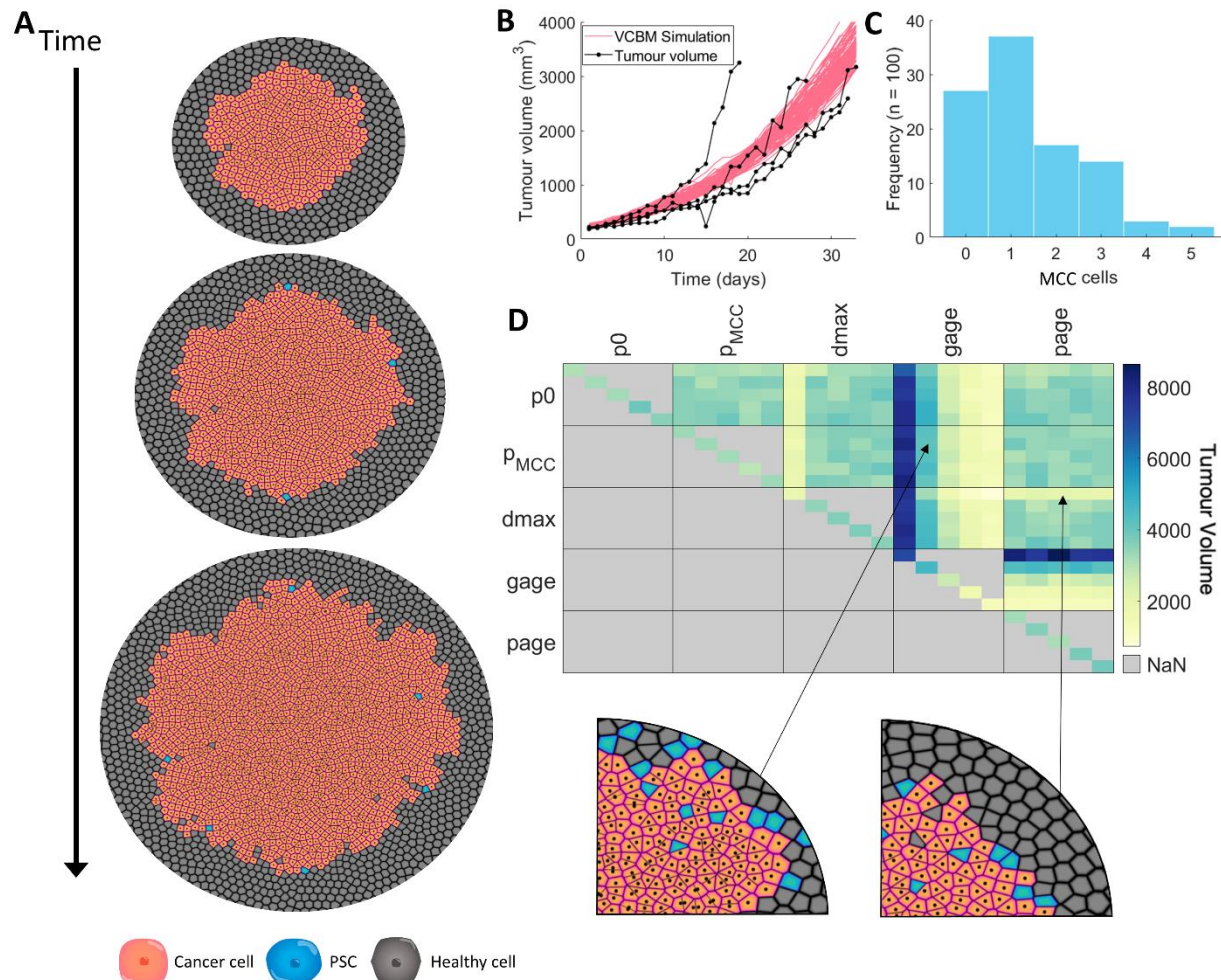
12

Figure 4 Using the VCBM to model control tumour growth. (A) Snapshots of the model simulation at 0, 5 and 10 days with cancer cells in orange, MCCs in blue and healthy cells in grey (a zoomed in version is in **Figure S6**). (B) Mia-PaCa-2 tumour volume over 33 days measured *in vivo* in mice (black, n=4). Overlaid is the tumour volume from the VCBM simulation (pink, n=100) with parameters from **Table S3**. (C) MCC counts in the VCBM simulations (n=100). (D) Sensitivity analysis of control tumour growth. Maximum tumour volume over 33 days for perturbations of parameters with weights of 0.25, 0.75, 1.25, 1.75 and 2.25, and spatial plots of large and small tumours simulated using the depicted weightings. In the heatmap, each pixel represents 30 averaged simulations with two parameters. In the boxes, the parameters vertically and horizontally in the grid are the weightings in ascending order, with each pixel being a "coordinate" representing the weighting for each parameter and the result from 30 averaged tests. Diagonal pixels only use individual parameters with different weightings.

sensitivity analysis. A systematic multi-parameter sensitivity analysis was performed for $p = [p_0, p_{MCC}, d_{max}, g_{age}, p_{age}]$ using weighting identified by Wells *et al.* [81] (**Figure 4**D). This sensitivity analysis can identify combinatorial influences of multiple parameters and elucidate systemic features of the model. The average tumour volume predicted by the model at day 33 for 10 simulations was recorded for each parameter set. Pairs of parameters were varied, with each cell of **Figure 4**D depicting the weighting applied to each parameter in p from 0.25, 0.75, 1.25, 1.75, and 2.25. This allowed for all combinations of alterations for two parameter values to be tested.

The time taken for a cell to prepare for mitosis, g_{age}, has the greatest impact on final tumour volume (**Figure 4**D). Increasing g_{age} decreases tumour volume and conversely a decrease in g_{age} increases the final volume. As a

13

389   result, the model predicts that if cells take longer to move through the cell cycle and undergo mitosis this will result

390   in a smaller tumour volume. Reducing the maximum distance, a cell can be from the periphery and still proliferate,

391   d_{max}, also appears to have a decreasing effect on the final tumour volume. This is to be expected, as reducing the

392   proliferating cell rim (through decreasing the distance from the periphery for which cells can proliferate) will reduce

393   the number of cells available to proliferate and subsequently reduce the tumour volume. Decreasing the value of d_{max}

394   only appears to have a significant impact on the final tumour volume when the weighting applied is $\leq 50\%$. In

395   comparison with d_{max} and g_{age}, the tumour volume is insensitive to changes in both the probability of a cell

396   proliferating if it has reached mitosis, p_0, and the probability of a new pancreatic cancer stem cell being created, p_{MCC}.

397   The time taken for a cell to reach adult size (when it can proliferate), p_{age}, similarly has a negligible impact on the

398   tumour volume.

399

400   *Intratumoural implantation provide an alternate effective protocol*

401   Before quantifying the efficacy of gemcitabine-loaded fibres, we first looked to evaluate the impact of single point

402   free-drug injections (**Figure 1**) of gemcitabine on the tumour volume. Simulating single point free-drug injections

403   with the VCBM-PDE is a simplification of the full model presented in **Eqs. (1)-(4)** where $F(r, y, t) = 0$. More details

404   on this can be found in the **Technical Supplementary Information**. We considered free-drug injections of

405   gemcitabine as administered along a radial axis of the tumour in either a single dose or four free-drug injections which

406   are rotationally symmetric (**Figure 5**A). In the case of the four injections, the total dosage is spread across the

407   injections so that the total amount of drug administered is conserved. Simulations of the model under the different

408   injection protocols can be found in **Figure 5**B-C and **Figure S7**. The sensitivity of parameter values governing tumour

409   volume were again probed, now under a single administration of gemcitabine at the centre of the tumour (**Figure 5**D-

410   E and **Figure S8**). The same trends with g_{age} and d_{max} were observed; however, an additional parameter, which

411   represents the concentration the drug required to have an impact on the tumour volume, IC_{50}, was found to influence

412   the volume under further perturbations of the parameter value (**Figure 5**E). As expected, a lower value of IC_{50}, which

413   indicates that a smaller concentration of the drug is required for it to influence cancerous cells, leads to a lower tumour

414   volume, while an increase leads to a higher tumour volume when compared to original estimate for IC_{50}.

415   To determine the effect of injection placement on tumour volume over time, five placements of a single

416   injection were considered at a distance d_m from the centre: a central injection ($d_m = 0$), and injections $d_m = 0.9$ mm

417   from the centre, $d_m = 1.7$ mm from the centre, $d_m = 2.5$ mm from the centre and $d_m = 3.5$ mm from the centre

418   (**Figure 5**A). For each of these placements, 30 simulations were run over 33 days and both the number of tumour cells

419   and the tumour volume over time were measured (**Figure 5**F). For a single injection, distance did not impact the

420   effectiveness of the injection and the tumour volume is qualitatively similar. There was a deviation from the consistent

421   standard deviation width for injections further from the tumour, but this can be attributed to the method used to

422   calculate the tumour volume in terms of how it deals with tumour structures which are not part of the central mass.

423   The tumour volume was more significantly affected by distance in the case of four injections (**Figure 5**F), with free-

424   drug injections further away from the centre of the tumour performing worse than those intratumoural injections.

425   Primarily, single free-drug injections implanted peritumourally may encourage branching of external tumour
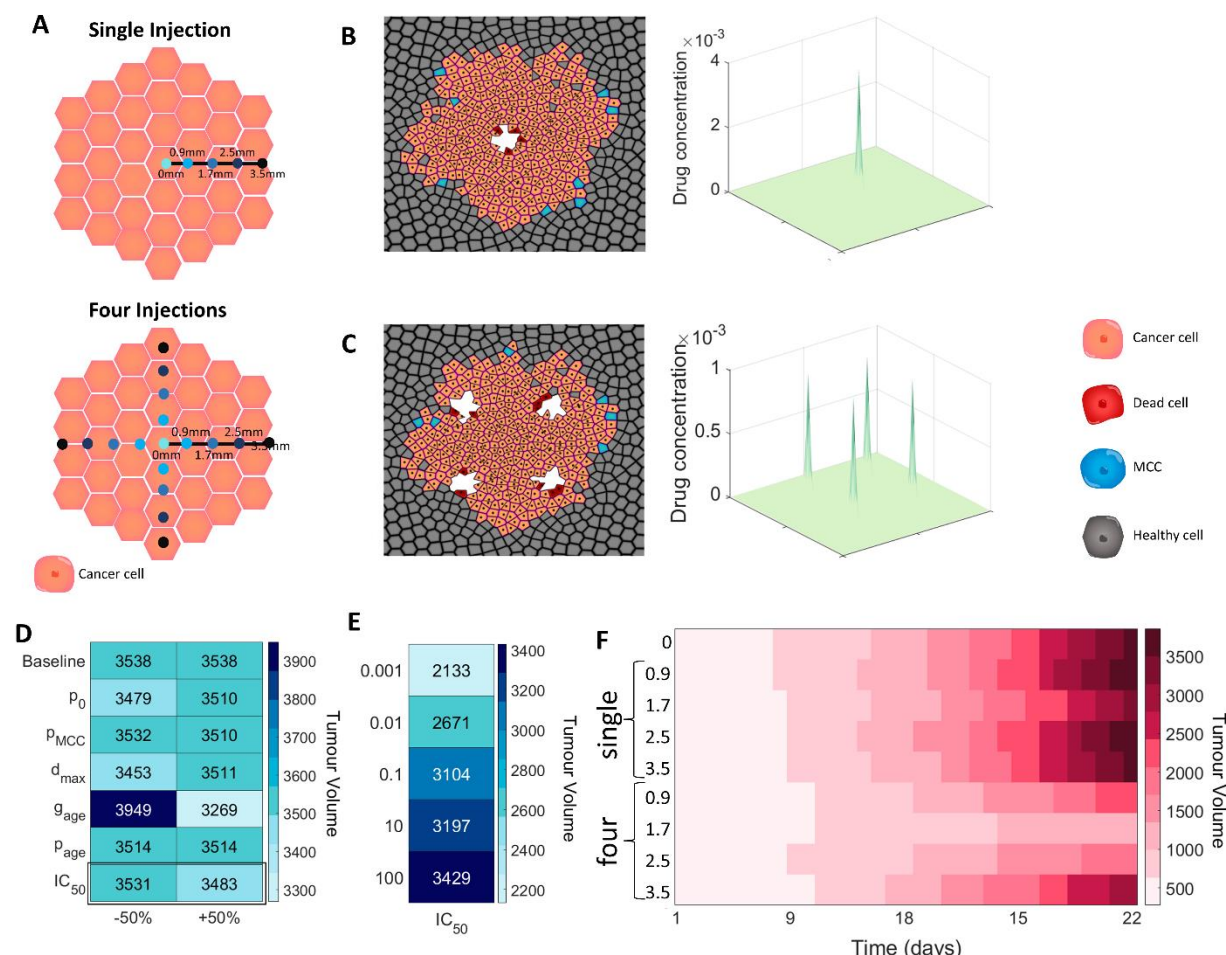
Figure 5 Impact of intratumoural free-drug point injections on tumour cell eradication. (A) Tumour growth was investigated under different gemcitabine single free-drug injections: central, 0.9 mm from centre, 1.7 mm from centre, 2.5 mm from centre, 3.5 mm from centre. Locations of injections on the tumour surface for single or four single free-drug injections is depicted schematically. (B) VCBM with a single central injection and the drug concentration at 24h. (C) The tumour volume with four injections placed $30\mu m$ from the centre, and the drug concentration at each location at 6h. (D) Maximum tumour volume over 33 days for $\pm 50\%$ perturbations in parameter values compared to the normal value (i.e. baseline parameter values). (E) Maximum tumour volume over 33 days for different perturbations of IC_{50} compared to the normal volume. (F) The tumour volume over 33 days with each injection protocol, averaged over 10 simulations.

structures in the model, and hence increase the calculated volume as it is based on the maximum distance from the centre of the tumour to the edge. While we present an approximation for tumour volume and placement of injections in units relevant to *in vivo* models (i.e. mm^3 and mm respectively), more work needs to be done to validate that the efficacy of treatment predicted by the model would map to the human scale.

Fibre location and release kinetics are a major driver of tumour arrest or tumour growth

Using the VCBM-PDE, we analysed the impact of varying the position of the fibre and the initial drug concentration on the tumour growth dynamics (**Figure 6**A). We introduced three classifications for the tumour growth dynamics: tumour eradication (i.e. a tumour volume <1mm^3) tumour stabilisation, i.e. a tumour volume at day 33 less than the initial tumour size (≈ 100mm^3), and tumour growth, i.e. a tumour volume on day 33 greater than the initial tumour

15

444 volume. Large concentrations of gemcitabine loaded into the fibre positioned at $d_m = 3.5$ mm or $d_m = 4.3$ mm from

445 the tumour centre were unable to stabilise or eradicate the tumour, also known as tumour arrest (**Figure 6**B-C and

446 **Figure S10**). Once the fibre was positioned closer to the tumour centre (≤ 1.7 mm) lower concentrations of drug were

447 sufficient to result in stabilisation of the tumour growth (**Figure 6**B). It was only with high drug concentration and

448 centered fibres that we saw complete tumour eradication (**Figure S9**). There are large variations in the response of

449 tumour growth to the different protocols, suggesting that tumour stabilisation or arrest might be achievable for some

450 tumours whereas others might experience tumour growth even in the presence of drug-loaded fibre.

451 To then analyse the effects of changes to the drug release profile on the tumour growth, we investigated four

452 different release profiles: constant release, exponential release, sigmoidal Emax/Imax release profiles [82–84] (See

453 the **Technical Supplementary Information, Section TS3**). Each of these release profiles were parameterised by a

454 release rate γ and for the Emax and Imax curves a half-effect term η. The different release profiles were tested with

455 the fibre placed either centrally (intratumourally) (**Figure 6**D) or on the periphery of the tumour (peritumourally)

456 (**Figure 6**E). The four different release profiles (constant, exponential, sigmoid emax, sigmoid imax) were tested with

457 8 different release rates. For each parameter value, 10 simulations were run over 33 days, with an initial amount of 500

458 μg of gemcitabine.

459 For fibres positioned in the centre (**Figure 6**D), it is possible to eradicate the tumour with all release profiles

460 considered given a small enough value of γ. In comparison, none of the drug release profiles resulted in tumour

461 eradication when positioned peripherally (**Figure 6**E). However, interestingly an exponential release profile with a

462 release rate of $\gamma = 10^{-4}$ results in the greatest decrease in tumour volume. This ideal release rate is likely because it

463 allows the drug concentration to remain in the therapeutic range and kill newly developed pancreatic cancer cells

464 aresting the process of cell proliferation. Comparing the drug release profiles (**Figure S11**), we see that the exponential

465 release rate is similar to the sigmoid release profiles, but slightly steeper initially, suggesting that a smooth release

466 rate with a sufficiently large initial drug release might be an optimal protocol to achieve a reduction in tumour size.

467

468 **Discussion**

469

470 PDAC is a difficult-to-treat cancer with a poor prognosis. Novel therapeutic interventions are desperately needed to

471 improve patient survival. While chemotherapy drugs, such as gemcitabine, have shown durable efficacy for pancreatic

472 cancer, there has been little to no improvement in patient survival in the last 30 years [85]. PDACs are notorious for

473 a dense fibrotic stroma that is interlaced with ECM [86] and is a major cause of therapeutic resistance [87]. One way

474 of improving drug retention at the tumour site, and by consequence increase tumour eradication and patient survival,

475 is through sustained-delivery devices (**Figure 1**). Polymeric fibres loaded with gemcitabine have shown increased

476 therapeutic efficacy over conventional treatment delivery. To further analyse the potential of these novel therapeutic

477 implants, we have designed a hybrid Voronoi cell-based model (VCBM)-partial differential equation (PDE) model to

478 describe pancreatic tumour formation in healthy pancreatic tissue and the resulting effect of gemcitabine on the tumour

479 tissue when delivered locally. With this model, we considered both the impact of a single fibre implanted with varying

480 drug release profiles and hypothesised alternative and more effective treatment protocols.
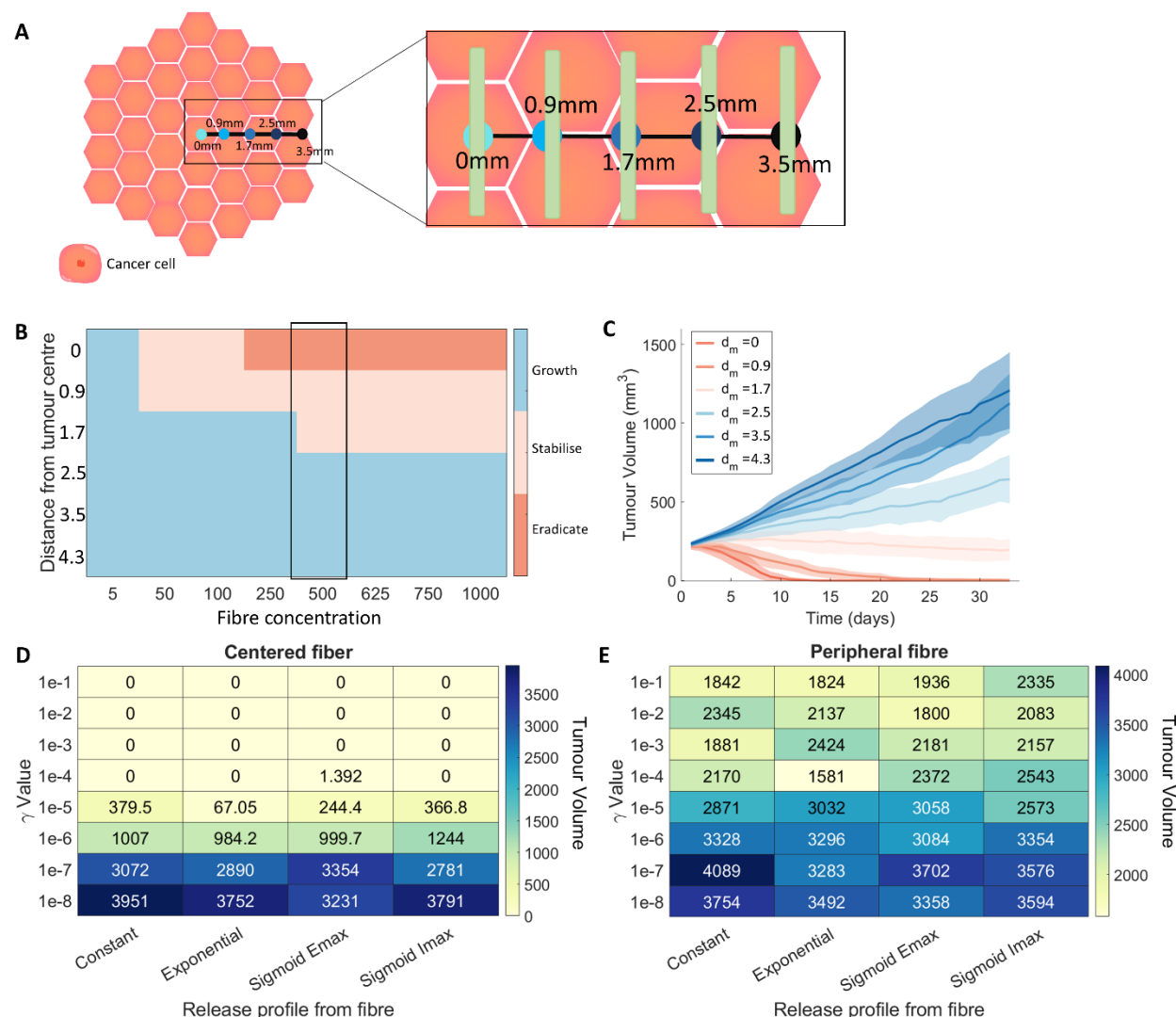
16

481

Figure 6 Comparison of different fibre release and placement options. (A) Tumour growth was investigated under different gemcitabine-loaded fibre placements d_m: central, 0.9 mm from centre, 1.7 mm from centre, 2.5 mm from centre, 3.5 mm from centre and 4.3 mm from centre. Locations of fibres on tumour surface for single implantations is depicted schematically. (B) A heatmap for the averaged final state of a tumour after 33 days of simulation for different initial injection concentrations and fibre placements. "Eradicate" denotes a tumour volume below $1mm^3$, "stabilise" denotes a tumour volume less than the initial tumour volume, and "growth" denotes a tumour volume greater than the initial tumour volume. (C) The mean (solid lines) and standard deviation (shades areas) of the tumour volume over 33 days for different fibre placement options with corresponding values highlighted in (B). (D) The tumour volume on day 33 for different release rates (indicated by the gamma value) and release profiles with a central fibre placement. (E) The tumour volume on day 33 for different release rates (indicated by the gamma value) and release profiles with a fibre placed on the edge of the tumour ($50\mu m$ away from centre). See **Section TS3** of the **Technical Supplementary Information** for more details on these release functions.

The model was calibrated to data and with these estimates, a parameter sensitivity analysis then revealed that the fundamental driver of tumour growth in our model was the rate of cell mitosis. The idea that the cell cycling time is a fundamental part of tumour progression has been found in other mathematical models [88], suggesting that the

495   model's sensitivity in terms of tumour volume is in line with other models in the literature. It is also known that
496   molecules can modulate the cell cycle of cancer cells, changing the cancer aggressivity. For example, melatonin is a
497   hormone known for its antitumour efficacy as it significantly increases the duration of the cell cycle of human breast
498   cancer cells [89]. Given a heterogeneous cohort of individuals with varying degrees of tumour growth rates, our model
499   suggests that the driver of these differences is most likely the cell cycling rate. Drugs targeting this should, therefore,
500   be considered.

501   Depending on the cancer type, administering an intratumoural injection of a drug can be extremely difficult
502   and administering treatments on the periphery can be an easier course of action. Simulating the model, we found that
503   intratumoural administration of gemcitabine-loaded fibres significantly outperforms peritumoural administration both
504   in terms of the number of fibres and fibre placement. However, there is a threshold distance from the tumour to achieve
505   an effective treatment, beyond which placing fibres further into the tumour bulk sees no added benefit. There is a
506   clear benefit to increasing the dosage multiplicity and spreading the administered drug out amongst the tumour
507   compared to a single high dose. Tumour volume was most significantly decreased when four free-drug point injections
508   were administered compared to a single free-drug point injection. This proposes the existence of a potential threshold
509   above which increasing the multiplicity of dosages or dosage size has a negligible effect over spreading out the
510   dosages.

511   The location of the fibre and the total drug concentration in the fibre was a major driver of tumour eradication.
512   For fibres located within the centre of the tumour with a significantly high drug concentration, it was possible to
513   completely eradicate the tumour. Moving the fibre farther away from the centre, we found that there was no
514   concentration of drug that would inhibit growth. This suggests that a large amount of drug from the implants is lost to
515   the surrounding tissue, and this has detrimental effects on the efficacy of these devices. Fortunately, simulations show
516   there is a minimal concentration of drug necessary for stabilisation, allowing these predictions to be used a way to
517   guide dosage so that toxicity is minimised and efficacy is maximised.

518   The release of the drug from the fibre has a major effect on the resulting tumour volume. Implementing an
519   exponential drug release profile, we were able to optimise the treatment to reduce the tumour size most significantly.
520   This suggests that an initial high dosage of drug followed by a slow decline in the drug release may be an optimal
521   protocol. This may be because it initiated a large amount of cell death initially, followed by a slower diffusion to reach
522   remaining viable cells. While exciting, an exponential release profile needs to be tested experimentally both for its
523   feasibility for the polymer release and to verify the predicted efficacy.

524   More recently, research has been focused on combining gemcitabine with other drugs to improve its efficacy.
525   Nanoparticle albumin-bound paclitaxel (nab-paclitaxel) administered in combination with gemcitabine [9] is one of
526   the standard of care treatment regimens that has shown an increase in overall survival in patients with advanced PDAC,
527   as shown in a Phase I/II clinical trial [9]. A phase III clinical trial showed that gemcitabine and erlotibin also
528   significantly increased overall survival in advanced PDAC patients compared to gemcitabine alone [90, 91].

529   Due to wanting to reduce the computational complexity of the VCBM, we made some simplifying
530   assumptions that have introduced limitations into our model. To avoid simulating excessively large numbers of cells,
531   we have chosen to scale the spatial unit appropriately so that we simulate on the order of $\sim 10^6$ cells. An improvement

532 for this model, could be to parallelise the agent update step to increase the speed of the simulation. In addition, we
533 consider only a 2-dimensional cross section of the tumour, which is a simplification given tumour's grow in 3-
534 dimensional environments. We feel that since we model neighbouring tissue as having a homogenous effect on tumour
535 growth, there would be no significant impact of extending our model to 3 dimensions. Lastly, we model cell uptake
536 by point sink terms; however, a cell would uptake drug across its surface area through drug molecule binding and
537 internalisation. It would be possible to model this by extending the framework from a single point uptake to a uniform
538 uptake across a cell's defined Voronoi cell region.

539 There are considerable avenues for future extensions of this work, and we feel the platform we have built is
540 easily extendable by other computational oncologists. In particular, future modelling could extend the model to
541 account for the dense fibrotic nature of PDAC [86, 87] and investigate the impact the release and delivery of drug. In
542 addition, the model could be used to simulate the efficacy of dual drug-loaded polymer and verify whether
543 improvements on the current treatment protocol exist. There are many applications of degradable polymeric drug
544 delivery systems in cancer therapy [10], for example, Rezk *et al.* [10] developed a pH-sensitive polymeric carrier to
545 study the local delivery of anticancer drug bortezomib. They fitted the release profile of the drug from their carrier
546 system to a mathematical formalism. Using our pancreatic cancer growth VCBM, it would be possible to feed in their
547 drug release mechanism and simulate the efficacy under alternative protocols and predict the remaining tumour
548 volume. Lastly, while we did not consider gemcitabine resistance in our model, it does occur in PDAC [3, 4]. A simple
549 extension of the model could consider the impact of resistance on the performance of therapy like other works on
550 resistance of chemotherapeutics using mathematical models [22, 92].

Conclusion

553 Treatment for cancers with a poor prognosis, such as PDAC, are in vital need of novel therapeutic approaches that
554 provide sustained, heightened, localised drug concentrations. The computational platform developed in this work can
555 recapitulate spatially heterogeneous tumour growth and treatment with the chemotherapy drug gemcitabine.
556 Investigating the efficacy of gemcitabine released from a degradable polymeric fibre implant, we are able to suggest
557 that a minimum dosage for maximum efficacy exists based on the location of the device within the tumour.
558 Furthermore, certain release profiles are significantly more effective than others, suggesting that the way in which
559 drug is released from these devices is crucial to improving patient treatment. Moving forward, a study of this form
560 could be used to help inform experimental design and be integrated into future device development.

References

1. Heinemann V (2001) Gemcitabine: progress in the treatment of pancreatic cancer. Oncology 60:8–18

2. Burris 3rd HA, Moore MJ, Andersen J, et al (1997) Improvements in survival and clinical benefit with gemcitabine as first-line therapy for patients with advanced pancreas cancer: a randomized trial. J Clin Oncol 15:2403–2413

3. Andersson R, Aho U, Nilsson BI, Peters GJ, Pastor-Anglada M, Rasch W, Sandvold ML (2009) Gemcitabine chemoresistance in pancreatic cancer: molecular mechanisms and potential solutions. Scand J Gastroenterol 44:782–786

4. Akada M, Crnogorac-Jurcevic T, Lattimore S, Mahon P, Lopes R, Sunamura M, Matsuno S, Lemoine NR (2005) Intrinsic chemoresistance to gemcitabine is associated with decreased expression of BNIP3 in pancreatic cancer. Clin Cancer Res 11:3094–3101

5. de Sousa Cavalcante L, Monteiro G (2014) Gemcitabine: metabolism and molecular mechanisms of action, sensitivity and chemoresistance in pancreatic cancer. Eur J Pharmacol 741:8–16

6. Cappella P, Tomasoni D, Faretta M, Lupi M, Montalenti F, Viale F, Banzato F, D'Incalci M, Ubezio P (2001) Cell cycle effects of gemcitabine. Int J cancer 93:401–408

7. Abrams MJ, Rakszawski K, Vasekar M, Passero F, Abbas A, Jia Y, Saif MW (2016) Recent advances in pancreatic cancer: Updates and insights from the 2015 annual meeting of the American Society of Clinical Oncology. Therap Adv Gastroenterol 9:141–151

8. Toschi L, Finocchiaro G, Bartolini S, Gioia V, Cappuzzo F (2005) Role of gemcitabine in cancer therapy.

9. Von Hoff DD, Ervin T, Arena FP, et al (2013) Increased survival in pancreatic cancer with nab-paclitaxel plus gemcitabine. N Engl J Med 369:1691–1703

10. Rezk AI, Obiweluozor FO, Choukrani G, Park CH, Kim CS (2019) Drug release and kinetic models of anticancer drug (BTZ) from a pH-responsive alginate polydopamine hydrogel: Towards cancer chemotherapy. Int J Biol Macromol 141:388–400

11. Nazir S, Khan MUA, Al-Arjan WS, Abd Razak SI, Javed A, Kadir MRA (2021) Nanocomposite hydrogels for melanoma skin cancer care and treatment: In-vitro drug delivery, drug release kinetics and anti-cancer activities. Arab J Chem 14:103120

12. Kearney CJ, Mooney DJ (2013) Macroscale delivery systems for molecular and cellular payloads. Nat Mater 12:1004–1017

13. Wade SJ, Sahin Z, Piper A-K, Talebian S, Aghmesheh M, Foroughi J, Wallace GG, Moulton SE, Vine KL (2020) Dual Delivery of Gemcitabine and Paclitaxel by Wet-Spun Coaxial Fibers Induces Pancreatic Ductal Adenocarcinoma Cell Death, Reduces Tumor Volume, and Sensitizes Cells to Radiation. Adv Healthc Mater 9:2001115

14. Wade SJ, Zuzic A, Foroughi J, Talebian S, Aghmesheh M, Moulton SE, Vine KL (2017) Preparation and in vitro assessment of wet-spun gemcitabine-loaded polymeric fibers: Towards localized drug delivery for the treatment of pancreatic cancer. Pancreatology 17:795–804

15. Lee KY, Mooney DJ (2012) Alginate: Properties and biomedical applications. Prog Polym Sci 37:106–126

16. Wade SJ (2019) Fabrication and preclinical assessment of drug eluting wet spun fibres for pancreatic cancer treatment.

17. Louzoun Y, Xue C, Lesinski GB, Friedman A (2014) A mathematical model for pancreatic cancer growth and treatments. J Theor Biol 351:74–82

18. Liu J, Wang XS (2019) Numerical optimal control of a size-structured PDE model for metastatic cancer treatment. Math Biosci 314:28–42

19. Lai X, Friedman A (2019) Mathematical modeling in scheduling cancer treatment with combination of VEGF inhibitor and chemotherapy drugs. J Theor Biol 462:490–498

20. Ghasemi M, Sivaloganathan S (2020) A computational study of combination HIFU–chemotherapy as a potential means of overcoming cancer drug resistance. Math Biosci 329:108456

21. Metzcar J, Wang Y, Heiland R, Macklin P (2019) A Review of Cell-Based Computational Modeling in Cancer Biology. JCO Clin Cancer Informatics 2:1–13

22. Craig M, Jenner AL, Namgung B, Lee LP, Goldman A (2020) Engineering in Medicine to Address the Challenge of Cancer Drug Resistance: From Micro: From Nanotechnologies to Computational and Mathematical Modeling. Chem Rev. https://doi.org/10.1021/acs.chemrev.0c00356

23. Gallaher JA, Enriquez-Navas PM, Luddy KA, Gatenby RA, Anderson ARA (2017) Spatial heterogeneity and evolutionary dynamics modulate time to recurrence in continuous and adaptive cancer therapies. bioRxiv 78:2127–2139

625 24. Gallaher JA, Massey SC, Hawkins-Daarud A, et al (2020) From cells to tissue: How cell scale heterogeneity
626   impacts glioblastoma growth and treatment response. PLoS Comput Biol 16:e1007672

627 25. Macnamara CK (2021) Biomechanical modelling of cancer: Agent-based force-based models of solid
628   tumours within the context of the tumour microenvironment. Comput Syst Oncol 1:e1018

629 26. Macnamara CK, Caiazzo A, Ramis-Conde I, Chaplain MAJ (2020) Computational modelling and simulation
630   of cancer growth and migration within a 3D heterogeneous tissue: The effects of fibre and vascular
631   structure. J Comput Sci 40:101067

632 27. Szymańska Z, Cytowski M, Mitchell E, Macnamara CK, Chaplain MAJ (2018) Computational Modelling of
633   Cancer Development and Growth: Modelling at Multiple Scales and Multiscale Modelling. Bull Math Biol
634   80:1366–1403

635 28. Phillips CM, Lima EABF, Woodall RT, Brock A, Yankeelov TE (2020) A hybrid model of tumor growth
636   and angiogenesis: In silico experiments. PLoS One 15:e0231137

637 29. Ozik J, Collier N, Wozniak JM, Macal C, Cockrell C, Friedman SH, Ghaffarizadeh A, Heiland R, An G,
638   Macklin P (2018) High-throughput cancer hypothesis testing with an integrated PhysiCell-EMEWS
639   workflow. BMC Bioinformatics. https://doi.org/10.1186/s12859-018-2510-x

640 30. Ghaffarizadeh A, Heiland R, Friedman SH, Mumenthaler SM, Macklin P (2018) PhysiCell: An open source
641   physics-based cell simulator for 3-D multicellular systems. PLoS Comput Biol 14:e1005991

642 31. Berg DR, Offord CP, Kemler I, Ennis MK, Chang L, Paulik G, Bajzer Z, Neuhauser C, Dingli D (2019) In
643   vitro and in silico multidimensional modeling of oncolytic tumor virotherapy dynamics. PLoS Comput Biol
644   15:1–18

645 32. Jenner AL, Frascoli F, Coster ACF, Kim PS (2020) Enhancing oncolytic virotherapy: Observations from a
646   Voronoi Cell-Based model. J Theor Biol. https://doi.org/10.1016/j.jtbi.2019.110052

647 33. Chen J, Weihs D, Vermolen FJ (2020) A Cellular Automata Model of Oncolytic Virotherapy in Pancreatic
648   Cancer. Bull Math Biol 82:1–25

649 34. Wodarz D, Hofacre A, Lau JW, Sun Z, Fan H, Komarova NL (2012) Complex spatial dynamics of oncolytic
650   viruses in vitro: mathematical and experimental approaches. PLoS Comput Biol 8:e1002547

651 35. Engeland CE, Heidbuechel JPW, Araujo RP, Jenner AL (2022) Improving immunovirotherapies: the
652   intersection of mathematical modelling and experiments. ImmunoInformatics 6:100011

653 36. Chen J, Vermolen FJ (2021) Several Agent-Based and Cellular Automata Mathematical Frameworks for
654   Modeling Pancreatic Cancer. In: Numer. Math. Adv. Appl. ENUMATH 2019. Springer, pp 265–274

655 37. Dogra P, Ram\'\irez JR, Peláez MJ, Wang Z, Cristini V, Parasher G, Rawat M (2020) Mathematical
656   modeling to address challenges in pancreatic cancer. Curr Top Med Chem 20:367–376

657 38. Arifin DY, Lee LY, Wang CH (2006) Mathematical modeling and simulation of drug release from
658   microspheres: Implications to drug delivery systems. Adv Drug Deliv Rev 58:1274–1325

659 39. Lao LL, Peppas NA, Boey FYC, Venkatraman SS (2011) Modeling of drug release from bulk-degrading
660   polymers. Int J Pharm 418:28–41

661 40. Siepmann J, Siepmann F (2012) Modeling of diffusion controlled drug delivery. J Control Release 161:351–
662   362

663 41. Casalini T, Rossi F, Lazzari S, Perale G, Masi M (2014) Mathematical modeling of PLGA microparticles:
664   From polymer degradation to drug release. Mol Pharm 11:4036–4048

665 42. McGinty S, King D, Pontrelli G (2017) Mathematical modelling of variable porosity coatings for controlled
666   drug release. arXiv 45:51–60

667 43. Jenner AL, Frascoli F, Yun CO, Kim PS (2020) Optimising hydrogel release profiles for viro-
668   immunotherapy using oncolytic adenovirus expressing IL-12 and GM-CSF with immature dendritic cells.
669   Appl Sci 10:2872

670 44. Kalkhoran AHZ, Vahidi O, Naghib SM (2018) A new mathematical approach to predict the actual drug
671   release from hydrogels. Eur J Pharm Sci 111:303–310

672 45. Manga RD, Jha PK (2017) Mathematical models for controlled drug release through pH-responsive
673   polymeric hydrogels. J Pharm Sci 106:629–638

674 46. Spiridonova TI, Tverdokhlebov SI, Anissimov YG (2019) Investigation of the Size Distribution for
675   Diffusion-Controlled Drug Release From Drug Delivery Systems of Various Geometries. J Pharm Sci
676   108:2690–2697

677 47. Ghaffarizadeh A, Friedman SH, MacKlin P (2016) BioFVM: An efficient, parallelized diffusive transport
678   solver for 3-D biological simulations. Bioinformatics 32:1256–1258

679 48. Petlin DG, Rybachuk M, Anissimov YG (2015) Pathway Distribution Model for Solute Transport in
680   Stratum Corneum. J Pharm Sci 104:4443–4447

49. Petlin DG, Amarah AA, Tverdokhlebov SI, Anissimov YG (2017) A fi ber distribution model for predicting drug release rates. J Control Release 258:218–225

50. Kaunisto E, Marucci M, Borgquist P, Axelsson A (2011) Mechanistic modelling of drug release from polymer-coated and swelling and dissolving polymer matrix systems. Int J Pharm 418:54–77

51. Pasdunkorale A J, Turner IW (2005) A second order control-volume finite-element least-squares strategy for simulating diffusion in strongly anisotropic media. J Comput Math 1–16

52. Chaudhry QA, Abbas A, Noor A, Asif M (2019) In silico modeling for the risk assessment of toxicity in cells. Comput \& Math with Appl 77:1541–1548

53. Shakeri F, Dehghan M (2011) The finite volume spectral element method to solve Turing models in the biological pattern formation. Comput \& Math with Appl 62:4322–4336

54. Andasari V, Gerisch A, Lolas G, South AP, Chaplain MAJ (2011) Mathematical modeling of cancer cell invasion of tissue: biological insight from mathematical analysis and computational simulation. J Math Biol 63:141–171

55. Hubbard ME, Byrne HM (2013) Multiphase modelling of vascular tumour growth in two spatial dimensions. J Theor Biol 316:70–89

56. Eymard R, Gallouët T, Herbin R (2000) Finite volume methods. Handb Numer Anal 7:713–1018

57. Khalid S, Chaudhry QA (2019) Quantitative analysis of cancer risk assessment in a mammalian cell with the inclusion of mitochondria. Comput \& Math with Appl 78:2449–2467

58. Ain K, Wibowo RA, Soelistiono S (2017) Modeling of electrical impedance tomography to detect breast cancer by finite volume methods. In: J. Phys. Conf. Ser. p 12001

59. Storey KM, Jackson TL (2021) An Agent-Based Model of Combination Oncolytic Viral Therapy and Anti-PD-1 Immunotherapy Reveals the Importance of Spatial Location When Treating Glioblastoma. Cancers (Basel) 13:5314

60. Haroske G, Dimmer V, Steindorf D, Schilling U, Theissig F, Kunze KD (1996) Cellular sociology of proliferating tumor cells in invasive ductal breast cancer. Anal Quant Cytol Histol 18:191–198

61. Bock M, Tyagi AK, Kreft J-U, Alt W (2010) Generalized voronoi tessellation as a model of two-dimensional cell tissue dynamics. Bull Math Biol 72:1696–1731

62. Saribudak A, Kucharavy H, Hubbard K, Uyar MÜ (2016) Spatial Heterogeneity Analysis in Evaluation of Cell Viability and Apoptosis for Colorectal Cancer Cells. IEEE J Transl Eng Heal Med 4:1–9

63. Lin L, Wang X, Zeng X (2014) Geometrical modeling of cell division and cell remodeling based on Voronoi tessellation method. C Comput Model Eng \& Sci 98:203–220

64. Saribudak A, Dong Y, Gundry S, Hsieh J, Uyar MÜ (2015) Mathematical models of tumor growth using Voronoi tessellations in pathology slides of kidney cancer. In: 2015 37th Annu. Int. Conf. IEEE Eng. Med. Biol. Soc. pp 4454–4457

65. Maier HJ, Wirth T, Beug H (2010) Epithelial-mesenchymal transition in pancreatic carcinoma. Cancers (Basel) 2:2058–2083

66. Luu T (2021) Epithelial-mesenchymal transition and its regulation mechanisms in pancreatic cancer. Front Oncol 11:1228

67. Karamitopoulou E (2013) Role of epithelial-mesenchymal transition in pancreatic ductal adenocarcinoma: is tumor budding the missing link? Front Oncol 3:221

68. Bulle A, Lim K-H (2020) Beyond just a tight fortress: contribution of stroma to epithelial-mesenchymal transition in pancreatic cancer. Signal Transduct Target Ther 5:1–12

69. Buijs JO den, Musters M, Verrips T, Post JA, Braam B, Van Riel N (2004) Mathematical modeling of vascular endothelial layer maintenance: the role of endothelial cell division, progenitor cell homing, and telomere shortening. Am J Physiol Circ Physiol 287:H2651--H2658

70. Lobo EP (2014) Modelling the Role of Interclonal Cooperativity During Early Carcinogenesis. University of Sydney

71. Kansal AR, Torquato S, Harsh GR, Chiocca EA, Deisboeck TS (2000) Simulated brain tumor growth dynamics using a three-dimensional cellular automaton. J Theor Biol 203:367–382

72. Jiao Y, Torquato S (2011) Emergent behaviors from a cellular automaton model for invasive tumor growth in heterogeneous microenvironments. PLoS Comput Biol 7:e1002314

73. Crosley P, Farkkila A, Jenner AL, et al (2021) Procaspase-Activating Compound-1 Synergizes with TRAIL to Induce Apoptosis in Established Granulosa Cell Tumor Cell Line (KGN) and Explanted Patient Granulosa Cell Tumor Cells In Vitro. Int J Mol Sci 22:4699

74. Kalvass JC, Pollack GM (2007) Kinetic considerations for the quantitative assessment of efflux activity and inhibition: implications for understanding and predicting the effects of efflux inhibition. Pharm Res 24:265–

22

276

75. Pena-Miller R, Laehnemann D, Jansen G, Fuentes-Hernandez A, Rosenstiel P, Schulenburg H, Beardmore R (2013) When the Most Potent Combination of Antibiotics Selects for the Greatest Bacterial Load: The Smile-Frown Transition. PLoS Biol 11:14–16

76. Minto CF, Schnider TW, Short TG, Gregg KM, Gentilini A, Shafer SL (2000) Response surface model for anesthetic drug interactions. Anesthesiology 92:1603–1616

77. Li Z, Tian T, Lv F, et al (2013) Six1 Promotes Proliferation of Pancreatic Cancer Cells via Upregulation of Cyclin D1 Expression. PLoS One. https://doi.org/10.1371/journal.pone.0059203

78. Sinha A, Cherba D, Bartlam H, Lenkiewicz E, Evers L, Barrett MT, Haab BB (2014) Mesenchymal-like pancreatic cancer cells harbor specific genomic alterations more frequently than their epithelial-like counterparts. Mol Oncol 8:1253–1265

79. Zhou P, Li B, Liu F, Zhang M, Wang Q, Liu Y, Yao Y, Li D (2017) The epithelial to mesenchymal transition (EMT) and cancer stem cells: implication for treatment resistance in pancreatic cancer. Mol Cancer 16:1–11

80. Chan T-S, Shaked Y, Tsai KK (2019) Targeting the interplay between cancer fibroblasts, mesenchymal stem cells, and cancer stem cells in desmoplastic cancers. Front Oncol 9:688

81. Wells DK, Chuang Y, Knapp LM, Brockmann D, Kath WL, Leonard JN (2015) Spatial and Functional Heterogeneities Shape Collective Behavior of Tumor-Immune Networks. PLoS Comput Biol. https://doi.org/10.1371/journal.pcbi.1004181

82. Upton RN, Mould DR (2014) Basic concepts in population modeling, simulation, and model-based drug development: Part 3-introduction to pharmacodynamic modeling methods. CPT Pharmacometrics Syst Pharmacol 3:1–16

83. Gabrielsson J, Andersson R, Jirstrand M, Hjorth S (2019) Dose-response-time data analysis: an underexploited trinity. Pharmacol Rev 71:89–122

84. Prinz H (2010) Hill coefficients, dose--response curves and allosteric mechanisms. J Chem Biol 3:37–44

85. Hardacre JM, Mulcahy M, Small W, Talamonti M, Obel J, Krishnamurthi S, Rocha-Lima CS, Safran H, Lenz H-J, Chiorean EG (2013) Addition of algenpantucel-L immunotherapy to standard adjuvant therapy for pancreatic cancer: a phase 2 study. J Gastrointest Surg 17:94–101

86. Perez VM, Kearney JF, Yeh JJ (2021) The PDAC Extracellular Matrix: A Review of the ECM Protein Composition, Tumor Cell Interaction, and Therapeutic Strategies. Front Oncol 4114

87. Xie D, Xie K (2015) Pancreatic cancer stromal biology and therapy. Genes \& Dis 2:133–143

88. Crivelli JJ, Földes J, Kim PS, Wares JR (2012) A mathematical model for cell cycle-specific cancer virotherapy. J Biol Dyn 6:104–120

89. Cos S, Recio J, Sánchez-Barceló EJ (1996) Modulation of the length of the cell cycle time of MCF-7 human breast cancer cells by melatonin. Life Sci 58:811–816

90. Conroy T, Hammel P, Hebbar M, et al (2018) FOLFIRINOX or gemcitabine as adjuvant therapy for pancreatic cancer. N Engl J Med 379:2395–2406

91. Moore MJ, Goldstein D, Hamm J, et al (2007) Erlotinib plus gemcitabine compared with gemcitabine alone in patients with advanced pancreatic cancer: a phase III trial of the National Cancer Institute of Canada Clinical Trials Group. J Clin Oncol 25:1960–1966

92. Cassidy T, Nichol D, Robertson-Tessi M, Craig M, Anderson ARA (2021) The role of memory in non-genetic inheritance and its impact on cancer treatment resistance. PLoS Comput Biol 17:e1009348